Turbulent point source plumes in confined, rotating environments

Christopher J. Howland

September 2018

1 Introduction

Turbulent buoyant plumes are prolific in geophysical and environmental flows. They exist over a wide range of scales, from the small wisps of smoke rising above a fire to the massive ash clouds from the eruption of a volcano. On the largest geophysical scales, both rotation and stratification affect the development of a plume. In some cases, plumes can be produced in regions of low stratification, and so rotation is thought to have a more dominant effect on their development. For example, plumes of dense water can be formed at high latitudes in regions of weak stratification due to sea ice formation [16]. Astrophysicists have also hypothesised that plumes produced at the base of the well-mixed subsurface ocean of Europa are affected strongly by rotation [11].

In the case of sea ice formation, one can think of multiple sources of dense water forming in the marginal ice zone which can lead to nearby plumes interacting with each other. The combined effects of interaction of the plumes and rotation on entrainment will control the amount of mixing that the dense water undergoes on its journey to the bottom of the ocean. The properties of this bottom water are thus closely linked to the plume dynamics, and understanding these external effects on the plume is important for gaining insight into abyssal water formation which helps drive the meridional overturning circulation.

Two previous research projects at the WHOI GFD Program have used laboratory experiments to investigate these problems. In 2009 Yamamoto, Cenedese and Caulfield performed experiments with a pair of axisymmetric, turbulent plumes in a rotating environment and varied the separation distance of the plume sources as well as the rotation rate. They focused on the early time behaviour of the plume and observed qualitative differences in the flow depending on whether the plumes merged before being affected by rotation or vice versa [22]. If the plumes merged at early times, a single cyclonic vortex was generated in the ambient fluid, whereas two vortices appeared if the rotation rate was sufficiently high.

The second project took a more systematic approach in order to quantify the effect on entrainment of the interaction of two plumes in a non-rotating frame. Cenedese and Linden [4] carried out experiments in 2013 based on the ventilated filling box technique first implemented by Baines (1983) [1]. They formulated and verified a simple model based on conservation of mass and self-similarity of merged plumes to compare the "effective" entrainment of the merging plumes against the entrainment that would occur from two independent plumes with the same source properties.

The development of a plume can also be affected by the presence of a nearby vertical boundary. The interaction of point source plumes with adjacent walls has been studied less than merging plumes, but still has important geophysical applications [5, 7, 19]. Following research on turbulent wall jets [14], turbulent plumes are expected to become asymmetric, spreading more across the wall than away from it. This is due to the creation of streamwise vorticity near the boundary when the no-slip condition is enforced. The effect of rotation on this problem has not yet been tested and is currently unknown.

The aim of this study is to use a similar type of filling box experiment to that in [4] to precisely quantify the effect of rotation on the entrainment of turbulent plumes. However we find that the lower boundary of the tank has a strong influence on the development of the filling box, making the measurement of entrainment from this method practically impossible. We also perform further experiments to investigate the effect of rotation on point source wall plumes, using the development of the plume shape to measure effects on dispersion and identify mechanisms by which the plume may *detrain* fluid.

The rest of this report is organised as follows. In section 2 the classical theory of point source, axisymmetric plumes will be introduced, followed by a brief overview of the existing literature on the effects of rotation and studies of turbulent wall plumes. We will then outline the experimental setups used for the various experiments in section 3, and delve deeper into the issues that hindered the filling box experiments. The results of the wall plume experiments will then be presented in section 4, before we finally discuss the implications of our findings and the potential avenues for future research in section 5.

2 Theory and literature

2.1 Classical plume theory

Many developments in the field of turbulent plumes have stemmed from the groundbreaking paper of Morton, Taylor and Turner (1956) [18]. They considered the axisymmetric, statistically steady state with plume radius $b(z)$ arising from a maintained source of constant buoyancy flux and made use of four key assumptions:

- self-similarity: the profiles of vertical velocity $u(z)$ and buoyancy $g'(z) = g(\rho_a - \rho(z))/\rho_0$ are the same at all heights;
- linear entrainment: the rate of entrainment of fluid is proportional to the vertical velocity at all heights ($u_e = \alpha u$);
- incompressibility: fluid does not change volume on mixing;
- the Boussinesq approximation holds: local variations in density are small compared to some reference density ($\rho - \rho_a \ll \rho_0$).

Using these assumptions, and further assuming 'top-hat' profiles for u and g', we can write down the following equations for conservation of volume, momentum and buoyancy

$$Q = \pi b^2 u, \qquad \frac{dQ}{dz} = 2\pi b \alpha u = 2\pi^{1/2} \alpha M^{1/2}, \tag{1}$$

$$M = \pi b^2 u^2, \qquad \frac{dM}{dz} = \pi b^2 g' = \frac{BQ}{M}, \tag{2}$$

$$B = \pi b^2 u g' \qquad \frac{dB}{dz} = 0, \tag{3}$$

where Q, M and B are volume flux, momentum flux and buoyancy flux. In the final equation, we have also assumed that the ambient fluid is homogeneous, i.e. ρ_a does not vary with height. These equations can be easily solved, revealing that the plume radius takes the form $b = \frac{6}{5}\alpha z$. The time-averaged shape of a plume therefore provides a measure of the entrainment coefficient α, which decades of experiments have found to be approximately constant and equal to 0.1 ± 0.01 [21].

An alternative method for inferring the entrainment rate of a turbulent plume was devised by Baines and Turner in 1969 [2]. As shown in figure 1, dense plume fluid injected from a point source will descend to the bottom of an enclosed container, spread out and form a front which will rise as the plume fluid fills the tank. By conservation of mass, the net volume flux at the height of the front must be zero and hence

$$Q = (A - A_p) w_f. \tag{4}$$

Here A and A_p are the cross-sectional areas of the tank and the plume respectively, w_f is the speed of the front, and Q is the volume flux of the plume. It is typically assumed that $A_p \ll A$, so Q can be computed just from measurements of the front speed. The

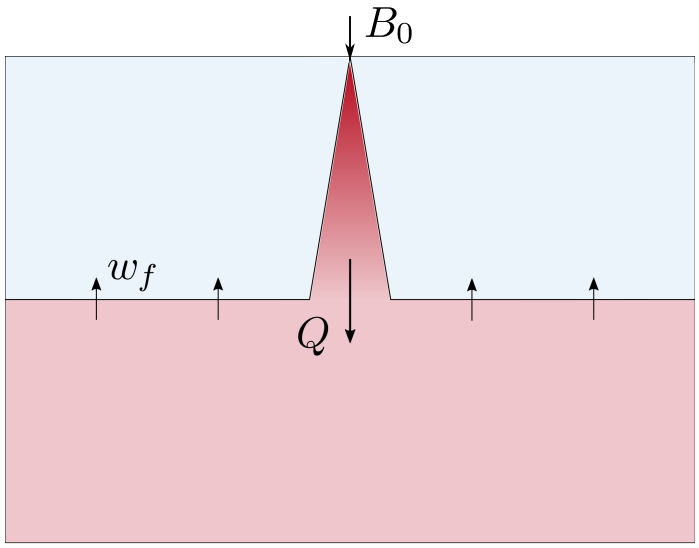

Figure 1: Schematic of a filling box experiment with a source of constant buoyancy flux B_0 as described in [2].

entrainment coefficient α can then be inferred from this measurement by comparing the observed variation of the volume flux with the prediction from classical theory:

$$Q = \left(\frac{9}{10}\right)^{1/3} \frac{6}{5}\pi^{2/3}\alpha^{4/3}B_0^{1/3}z^{5/3}. \tag{5}$$

Baines later improved the accuracy of measuring the volume flux in this way by ventilating the tank [1]. This was done by adding a source of constant volume flux to the upper ambient fluid and pumping fluid out of the bottom of the tank at the same rate. In this setup, the interface between the ambient fluid and the mixed fluid will move to and remain at an equilibrium height where the volume flux in the plume is precisely the volume flux being added to and removed from the tank. By adjusting the rate at which fluid is pumped in or out of the tank, it is possible to accurately measure the volume flux in the plume at all heights. One further advantage of this technique is that the two-layer stratification can be set up before the plume is running, resulting in a sharper front. This type of experiment was used by Cenedese and Linden in their study on merging plumes [4].

2.2 The effects of rotation

Many simple results in classical plume theory can be obtained by dimensional analysis, noting that the only conserved quantity is the buoyancy flux B_0, which has dimensions L^4T^{-3}. The steady state plume dynamics are well described by scaling laws that come about from combining B_0 and the local height z. When ambient rotation is non-negligible a new timescale is introduced to the problem, namely the inertial period of rotation $T_f = 2\pi/f$ where f is the Coriolis parameter. The introduction of f also suggests the importance of a new length scale $L_f = (B_0/f^3)^{1/4}$. Identifying how these scales affect the dimensional analysis requires experimental data. The Coriolis force will also strongly affect the plume dynamics directly as follows. For a non-rotating plume, entrainment draws ambient fluid towards the plume. When rotation is added, the Coriolis force acts on this motion in the ambient fluid, deflecting the flow into a cyclonic circulation (if $f > 0$) around the plume.

A number of experimental and numerical studies have been performed to gain insight on the effect of rotation on turbulent plumes and quantify the importance of these processes and scales [8, 9, 10, 11, 12, 20, 22]. Of the laboratory studies, Fernando, Chen and Ayotte (1998) were the first to investigate the development of a plume in a rotating but unstratified fluid [9]. They found that rotational effects become important after a time $0.764T_f$, before which the plume behaves as if no rotation is present. After $1.75T_f$, the lateral growth of the plume is restricted and the plume reaches a maximum width of $b_c \approx 2.35L_f$. This restriction implies that there is *no* entrainment below a certain height of the plume, which we had hoped to verify with our own experiments.

When the plume reached the bottom of the tank, Fernando et al. observed more interesting behaviour. As plume fluid continues to be injected, the plume spreads radially inducing an anticyclonic circulation near the base of the tank. After some time, this eddy reaches a size where it becomes baroclinically unstable and sheds from the main structure of the plume. This behaviour was also observed in an earlier study where the ambient was stratified, and the plume spread out above the neutral height rather than the solid boundary [12].

Lateral deflection of the plume was also observed, but not explained in the Fernando et al. study. It is now thought that the deflection of the plume is in fact regular, anticyclonic precession [8, 10]. Frank et al. (2017) performed experiments with a plume in a rotating, homogeneous ambient for a wide range of buoyancy fluxes, rotation rates, and water depths, finding that after one rotation period the plume moves about the vertical axis at a precession frequency of $\omega \approx 0.2f$. Fascinatingly, this frequency appears to be independent of the source size, buoyancy flux or water depth, implying that if rotation is present, it will always affect the dynamics.

2.3 Wall plumes

Turbulent wall plumes are often studied in the context of natural ventilation or melting glaciers [15, 17]. However, these papers usually consider the effect of a vertically distributed or planar source of buoyancy rather than a point source. Motivated by the plumes that rise up from subglacial meltwater channels along the side of a glacier, recent studies have modified the classical plume equations (1)-(3) to account for the effect of an adjacent wall [5, 7, 19]. By modifying the geometry to a half-cone and adding a quadratic drag force along the wall, the plume equations become

$$Q = \frac{\pi b^2}{2} u, \qquad \frac{dQ}{dz} = \pi b \alpha u = \sqrt{2\pi}\alpha M^{1/2}, \tag{6}$$

$$M = \frac{\pi b^2}{2} u^2, \qquad \frac{dM}{dz} = \frac{\pi b^2}{2} g' - 2c_d b u^2 = \frac{BQ}{M} - \frac{2^{3/2} c_D}{\sqrt{\pi}} \frac{M^{3/2}}{Q}, \tag{7}$$

$$B = \frac{\pi b^2}{2} u g' \qquad \frac{dB}{dz} = 0. \tag{8}$$

Despite the changes to the equations, the far-field asymptotic solution for the velocity follows the same scaling as the classical theory but has an extra pre-factor to account for the drag [7].

The effect of rotation on these wall plumes is currently unknown. Since the entrainment of a wall plume is asymmetric and the net flow induced by entrainment is towards the wall, the Coriolis force will generate a cross-flow along the wall when rotation is present. Purely due to geometrical constraints, there is potential for the precession observed in rotating plumes to be suppressed by the presence of the wall, and the lack of ambient circulation may affect the growth and breakup of baroclinic eddies.

3 Experimental setup

3.1 Filling box experiments

The laboratory setup of the initial filling box experiments is shown in the schematic of figure 2. A transparent, cubic tank of dimensions $60\text{cm} \times 60\text{cm} \times 60\text{cm}$ was filled to a depth of approximately 50cm with fresh water of density $\rho_a = 0.998\text{g}\,\text{cm}^{-3}$. The tank was placed on a rotating table which was rotated at Coriolis parameters of $f = 0\text{s}^{-1}$, $f = 0.5\text{s}^{-1}$ and $f = 1\text{s}^{-1}$. The table was spun up for at least 30 minutes before each experiment to ensure that the fluid in the tank was very close to solid body rotation. Filtered seawater of density

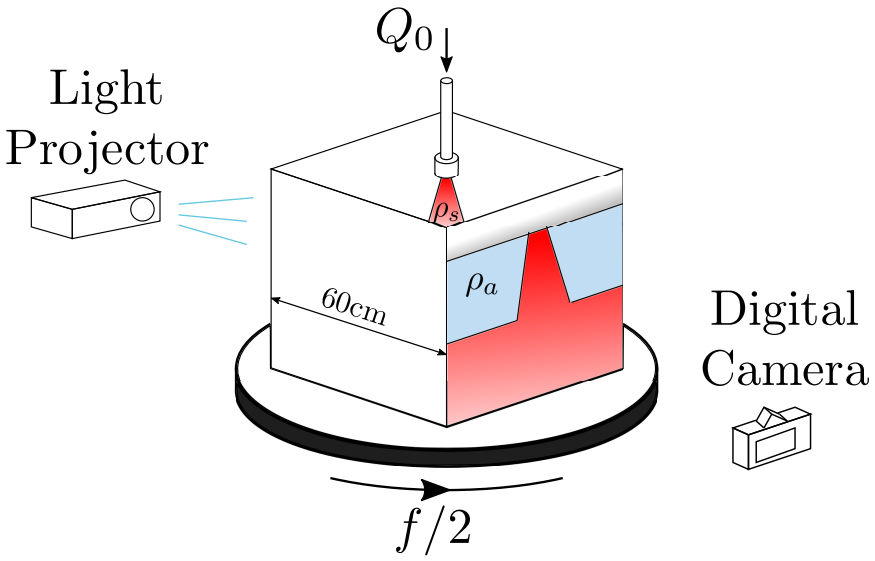

Figure 2: Schematic of the filling box setup.

$\rho = 1.02\mathrm{g\,cm^{-3}}$ was injected through a Cooper nozzle[1] of radius 2.65mm that was placed just below the surface of the water. A gear pump was used to pump the seawater through the nozzle at a constant volume flux Q_0, which was varied between 1 and $2\mathrm{cm^3\,s^{-1}}$ for different experiments. This gave a range of buoyancy fluxes of $B_0 = 20 - 40\mathrm{cm^4\,s^{-3}}$.

The seawater was dyed using red food dye so that the plume could be visualised easily using a shadowgraph technique. A light projector illuminated the experiment, and was placed approximately 2m away from the edge of the tank to prevent parallax issues in visualisation. One face of the tank was covered with a translucent sheet of paper to act as the recording plane for the shadowgraph. The experiment was recorded by an Olympus OM-D E-M10 Mark II digital camera attached to a tripod approximately 2m from the tank, directly opposite the light projector. Since neither the camera nor the projector were rotating with the tank, only one frame per rotation period could be used for analysing the experiment.

3.2 Filling box issues

In the non-rotating filling box experiments, the videos were processed as follows to obtain an entrainment coefficient α and a virtual origin correction z_0. In the regions to the left and right of the plume, the height of the front was determined in each pixel column by a threshold value for the reduction in blue light intensity. This height was then averaged across the pixel columns in each frame to obtain a time series for the front height $z_f(t)$. A polynomial fit was then used to interpolate the data, and this was numerically differentiated to give a front speed $w_f(t)$ and in turn a volume flux $Q = Aw_f$. Since the front height is known at all times, Q can also be plotted as a function of z. Rearranging (5) and accounting

[1]This type of nozzle uses a recirculation chamber and wire mesh to ensure turbulent outflow, and was first designed by Professor Paul Cooper, University of Wollongong, Australia.

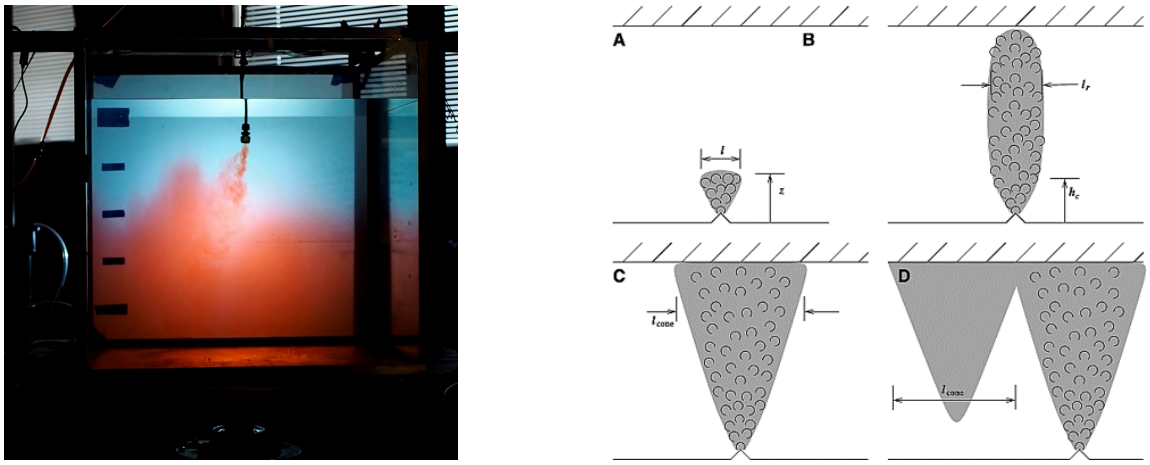

(a) (b)

Figure 3: (a) A picture of the experiment running with $f = 0.5$, showing plume deflection and a cone of dyed fluid indicative of a baroclinic eddy or possibly a 'heton'. (b) Schematic from Goodman et al. (2004) [11]: "Stages in the evolution of a buoyant convecting plume. A: Free turbulent convection. B: rotationally controlled cylindrical plume. C: Baroclinic cone. D: Baroclinic instability."

for a virtual origin gives

$$z = \alpha^{-4/5} \left(\frac{Q}{c_1 B_0^{1/3}} \right)^{3/5} - z_0, \tag{9}$$

where $c_1 = \left(\frac{9}{10}\right)^{1/3} \frac{6}{5}\pi^{2/3}$. Thus α and z_0 can be estimated by a linear fit for the above equation. Typical values computed for these parameters were $\alpha = 0.12$ and $z_0 = 1$cm.

Figure 3a highlights some of the difficulties in applying this method to the case of rotating plumes. Firstly the plume can be seen to deflect due to the precession identified in [10], which makes identifying regions over which to average a front height more challenging. Of greater concern is the shape of the front itself. The fact that there is not a clear, horizontal boundary between the dyed fluid and the clear ambient implies that the assumption of uniform upflow required for the filling box experiment is not valid. The mound of fluid that can be seen to the left of the plume propagates around the tank and is reminiscent of the anticyclonic eddies mentioned in section 2.2 and observed in previous studies [9, 11, 12]. Helfrich and Battisti (1991) suggest that the combination of this anticyclonic eddy with the cyclonic flow around the plume forms a 'heton' [12]. This term was first used by Hogg and Stommel (1985) to describe a pair of counter-rotating geostrophic vortices across a density interface which becomes pulled up or down depending on the sign of the vortices. [13]. Goodman et al. (2004) simply associate the shedding of a cone structure (as shown in figure 3b) with spreading of the dense fluid to a scale comparable to the Rossby radius of deformation $r_D = \sqrt{g'H}/f$, where H is the water depth [11].

Regardless of the origin of the tall cone of fluid, its presence in all of the rotating experiments makes the use of a filling box measurement to infer entrainment impossible. This

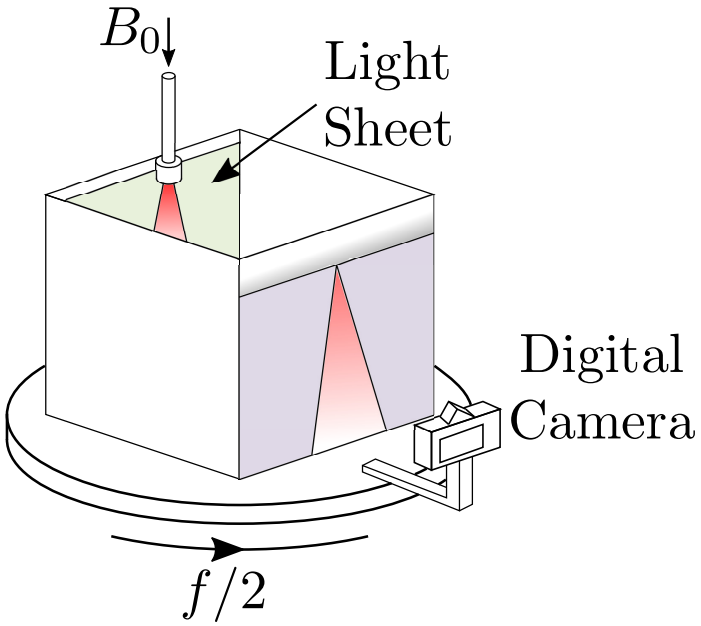

Figure 4: Schematic of the wall plume experimental setup when capturing the front view development of the wall plume.

led us to attempt an alternative experimental setup. Inspired by [3], where instantaneous measurements from a simple shadowgraph of the plume were used to determine properties of the mean flow, we prepared a setup similar to that shown in figure 4, but with the plume far from the boundaries of the tank. Unfortunately the observed plume precession prevented accurate measurement of the plume width and hence hindered us from obtaining useful statistics of the flow. Qualitatively it was interesting to observe *detrainment* of plume fluid into the ambient at all heights, although this exacerbated the problem of detecting the edge of the plume. Further investigation of the flow field in a rotating plume is needed to shed light on this behaviour. One possibility is that the detrainment could be related to the combination of the rigid boundary at the bottom of the tank and the Taylor–Proudman theorem, which together would hinder vertical motion in a rotating frame.

3.3 Wall plume experiments

The second experimental setup, used to investigate point source wall plumes in a rotating environment, is shown in figure 4. In contrast to the previous setup, both the digital camera and light source were attached to the rotating table to allow for a greater time resolution of 25fps in videos of the experiment. A projector and translucent sheet were not used for these experiments. Instead, electroluminescent Light Tape® attached to one face of the tank provided a uniform light source. The digital camera was attached to an arm on the rotating table approximately 60cm from the edge of the tank. Since we were only interested in the fluid near the plume, and not the entire width of the tank, the shorter distance between the camera and the tank edge did not lead to issues with parallax.

The same tank was used as in the filling box experiments, again filled with approximately

Volume flux Q_0 [$\mathrm{cm}^3\,\mathrm{s}^{-1}$]	Source density ρ_s [$\mathrm{g}\,\mathrm{cm}^{-3}$]	Coriolis parameter f [s^{-1}]
$2 - 2.5$	$1.02, 1.05$	$0, 0.5, 1, 2$

Table 1: Parameter values used for the wall plume experiments.

50cm of fresh water. For half of the wall plume experiments, extra salt was added to the seawater to increase its density, thus changing the buoyancy flux without altering the volume flux or momentum flux. A density meter measured the density of both the ambient fresh water and the source fluid before each experiment. The full range of parameter values used in the experiments can be found in table 1.

The plume source was attached to the illuminated side of the tank using filament tape such that the plume was directed vertically down the wall. The nozzle was placed a short distance below the surface of the water and halfway along the length of the wall to avoid the effect of the other boundaries of the tank. This setup provided a visualisation of the 'front view' describing how the plume spread along the wall. However due to the asymmetric development of wall plumes, we needed to repeat each experiment to also obtain a 'side view' showing how the plume spread away from the wall. For this setup, the plume source was attached to one of the walls adjacent to the illuminated side and the camera was moved so that it captured a view down that wall. Extra perspex sheets were added along the side with the plume to ensure that the view down the inner wall was not obscured by the corner of the tank.

The videos produced during the experiments were analysed using bespoke MATLAB scripts. Since the red dye concentration is linked to the reduction in blue light intensity, frame-by-frame analysis of the videos allows us to determine vertical profiles of the instantaneous width of the plume. The edges of the plume were defined at each height by locating the longest sequence of pixels where the blue light intensity was less than a given tolerance level. This tolerance was computed to be 80% above the minimum blue light intensity at each height relative to the background (maximum) light intensity.

4 Results

Due to the size and shape of the nozzle, the plume fluid did not exit the source attached to the boundary in the wall plume experiments. However since entrainment induces areas of low pressure surrounding the top of the plume, the ambient pressure away from the wall pushes the plume onto the wall. This is known as the Coandă effect, which leads to the plume becoming attached to the wall within the top few centimetres. In the non-rotating experiment, once the plume was attached to the wall it remained attached for the duration of its descent to the bottom of the tank. The plume developed into a steady state where the width measured along the wall (in front view) was a linear function of height. The leftmost panel of figure 5 shows the instantaneous width of the plume over a 3 minute time window of the experiment. This shows that the instantaneous profiles never deviate significantly from the mean. The gradient of the instantaneous half-width db_x/dz was found to be approximately 0.184, which is larger than typical values for unconfined plumes and suggests increased along-wall entrainment.

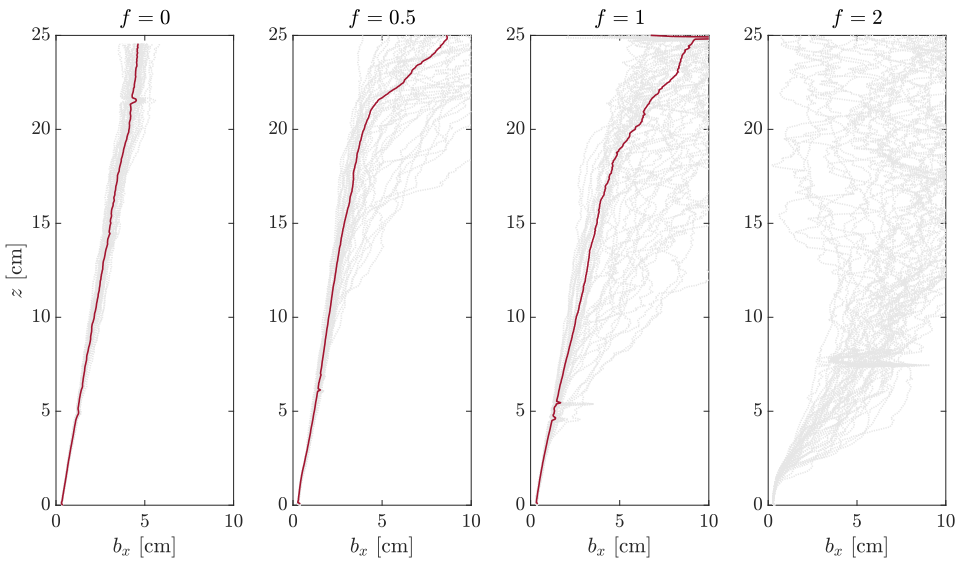

Figure 5: Vertical profiles of instantaneous plume half-width along the wall (in front view) over the course of four experiments with a volume flux of $Q_0 = 2\text{cm}^3\,\text{s}^{-1}$ and source density of $\rho_s = 1.023\text{g}\,\text{cm}^{-3}$. Profiles are only plotted for $t > 30$s to ignore the initial transient features of the plume. Each width is also averaged over 4s time intervals of 100 frames to smooth the data. Red lines indicate the time-mean of the instantaneous profiles that are considered to be in a 'quasi-steady' state.

The side view reveals that the steady state of the point source wall plume is unsurprisingly asymmetric. The vertical profile of the plume width away from the wall is however not a simple linear profile. Instead, the plume spreads out quickly within the top 3-4cm before descending with an almost constant width from the wall, as seen in the leftmost panel of figure 6. The fast spreading towards/away from the wall near the source may be attributed to Coandă-like effects which seem to be dominant in this region. The growth of turbulent eddies that engulf and entrain ambient fluid in a plume could be reduced in the direction perpendicular to the wall purely due to confinement. This would explain a reduction in entrainment away from the wall, but not the constant-width shape of the plume. One possibility is that the fluid entrained towards the wall squeezes the plume against the wall, leading to further spreading *along* the wall instead of growth away from it. This would be consistent with the generation of streamwise vorticity near the boundary observed for turbulent wall jets with no buoyancy [14].

Figures 5 and 6 compare the vertical profiles obtained at different rotation rates for a fixed volume flux and buoyancy flux. At early times and intermittently throughout the experiment, the plumes in rotating frames with $f = 0.5$ and $f = 1$ resemble the steady state found in the non-rotating experiment. We refer to the plume as being in a 'quasi-steady' state during these times, which can be identified as periods in which the fluctuations of the width in time are small. In figure 5, a fraction of the instantaneous profiles in grey for $f = 0.5$ and $f = 1$ are concentrated around an approximately linear profile associated with this quasi-steady state. The red lines are obtained by taking a time-mean of the profiles

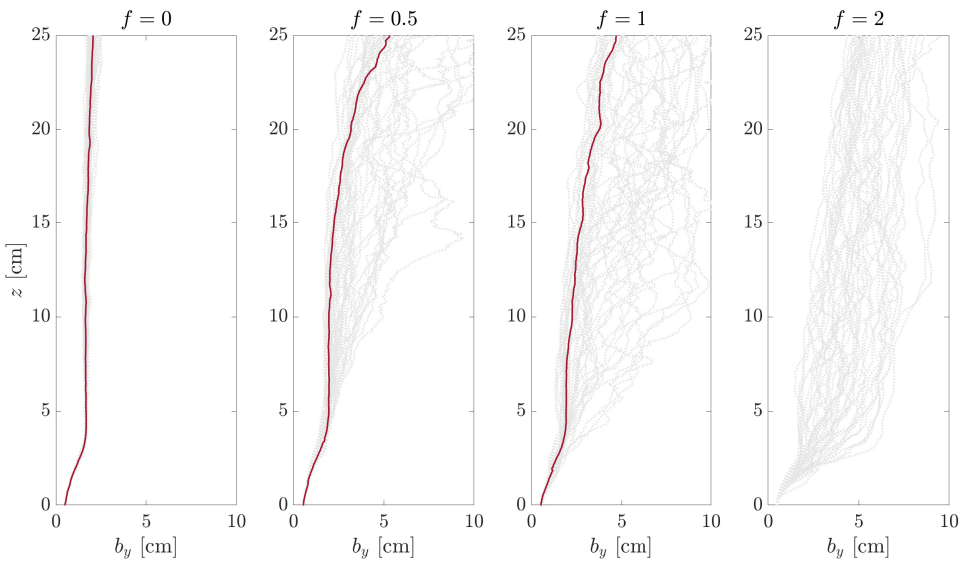

Figure 6: Vertical profiles of instantaneous plume width away from the wall (in side view) similar to figure 5. These experiments had an initial volume flux of $Q_0 = 2.15\text{cm}^3\,\text{s}^{-1}$.

considered to be in the quasi-steady state, and these profiles have similar gradients to the non-rotating steady state ($db_x/dz \approx 0.177$ for $f = 0.5$ and $db_x/dz \approx 0.2387$ for $f = 1$). The increase in gradient for $f = 1$ may simply be due to detraining dyed fluid making it hard to identify the edge of the plume. Beyond a certain distance from the source, the plume is not consistent with a linear profile and this distance reduces as the rotation rate increases. Bottom boundary effects becoming more important as rotation increases may explain these shrinking quasi-steady regions. At $f = 2$ no quasi-steady behaviour is observed, as can be seen in the rightmost panels of figures 5 and 6.

The vertical profiles from the side view in figure 6 have similar properties to those from the front view. At intermittent times throughout the experiments for $f = 0.5$ and $f = 1$, the plume exhibits a quasi-steady state but its connection to the non-rotating steady state is a little different. Both experiments show a rapid spreading near the source as in the non-rotating case which stops at a width just below 2cm. Moving vertically away from the source, the quasi-steady profile has a region where the width remains approximately constant before further spreading occurs. The size of the region of constant width decreases with rotation rate, again indicative of increasingly important bottom boundary effects.

Inspecting video snapshots from the experiments provides us with some understanding of the plume dynamics during the times when it is not in a quasi-steady state, and reveals remarkable quasi-periodic behaviour. As shown in figures 7b and 7d, the upper section of the plume occasionally detaches fully from the wall and moves to the left in the front view. This intriguingly means that the plume moves in the opposite direction along the wall to the cross flow that is induced by entrainment. After a short period of time being detached from the wall, the plume typically reattaches to the wall and adjusts back to the quasi-steady state seen in figures 7a and 7c. In the detached state, the upper plume fluid appears to become arrested at a certain height from the souce, and figure 7b also shows

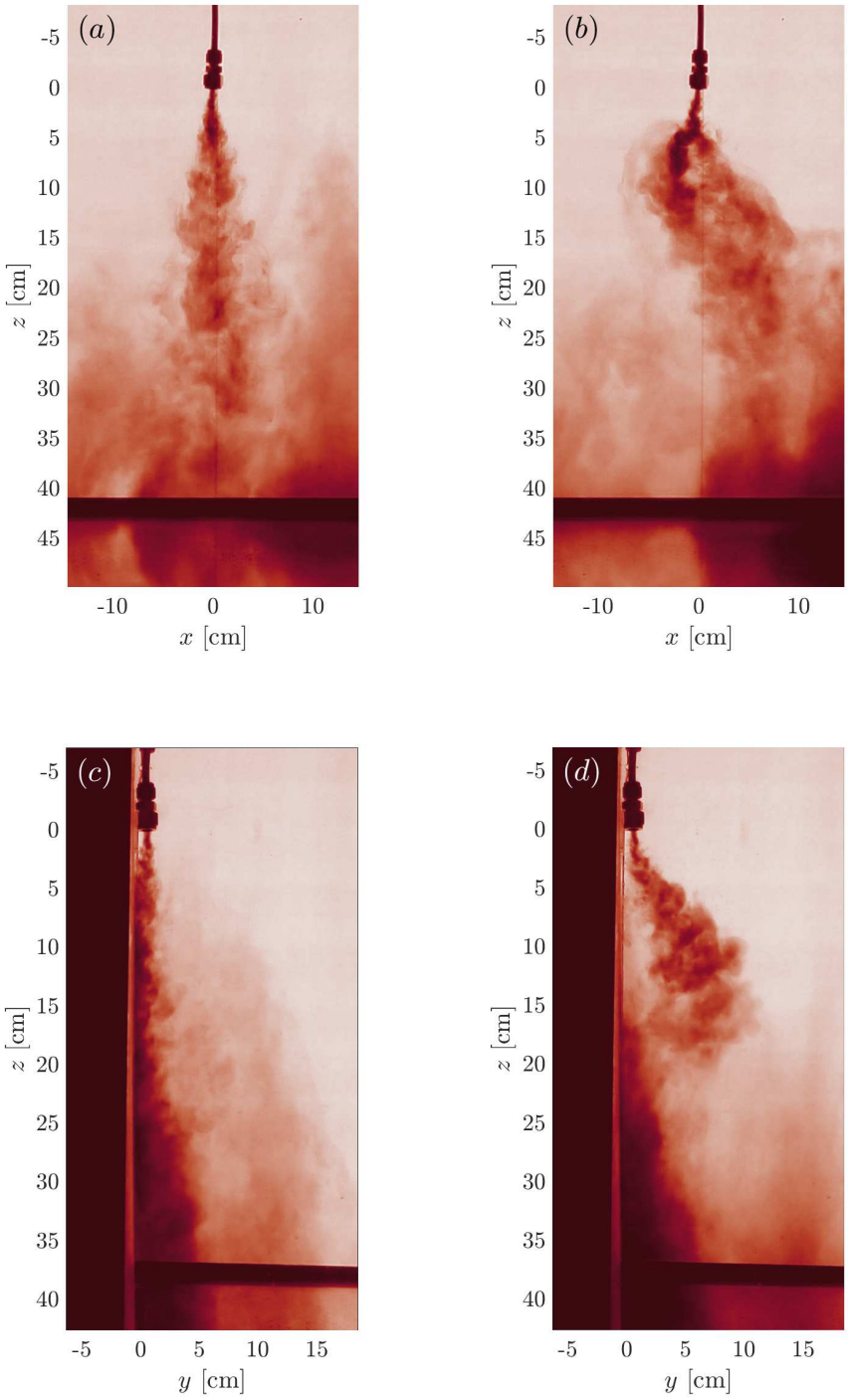

Figure 7: False colour images of blue light intensity from two experiments rotating at $f = 1$ with a source density of $\rho_s = 1.023\mathrm{g\,cm^{-3}}$. (a) and (b) show the front view at times $t = 60\mathrm{s}$ and $t = 100\mathrm{s}$ respectively for volume flux $Q_0 = 2\mathrm{cm^3\,s^{-1}}$. (c) and (d) show the side view (flipped left to right) at times $t = 50\mathrm{s}$ and $t = 80\mathrm{s}$ respectively for volume flux $Q_0 = 2.15\mathrm{cm^3\,s^{-1}}$.

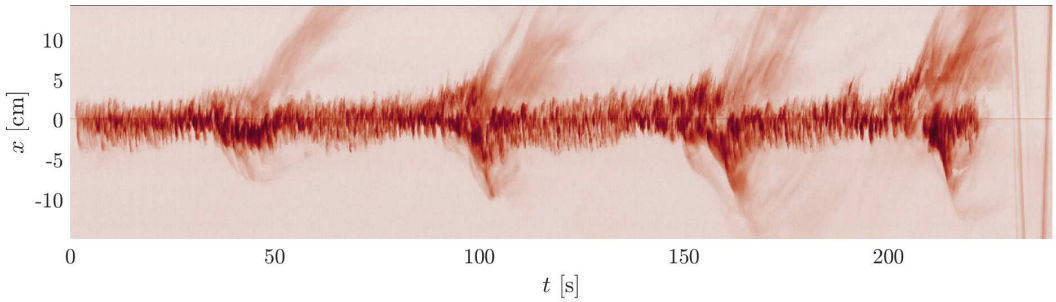

Figure 8: Time series of a horizontal slice of blue light intensity 10cm below the source level in front view for the same experiment as figures 7a and 7b.

that plume fluid further from the source is advected to the right along the wall. Videos of the experiment show that significant amounts of the fluid moving to the right is detrained from the plume while it is detached from the wall. This is clearly visualised in figure 8 by a time series of a horizontal slice 10cm below the plume. Large, diffuse patches propagating upwards in this figure correspond to fluid detraining to the right, and these coincide with the sudden deflections of the darker region associated with the plume.

A similar analysis for the side view experiment is shown in figure 9, which presents a time series of a vertical slice against the wall. The light space at the top of the figure shows that the plume does not leave the source attached to the wall and adjusts over a distance of 1-2cm. Detachment events can be seen clearly in figure 9 as the lighter patches descending over time. Although the front view and side view experiments were run with comparable parameters, the times of detachment are not consistent, suggesting that the mechanism is very sensitive to the experimental conditions or somewhat chaotic. This makes it difficult to determine whether the buoyancy flux has any effect on the frequency of detachment, but there is a clear trend for increasing rotation rate to increase the frequency of detachment as shown by figure 10.

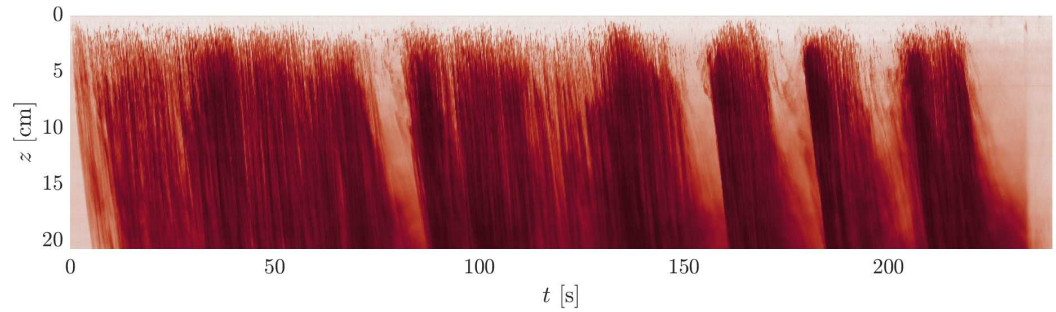

Figure 9: Time series of a vertical slice of blue light intensity between the source and the wall from the side view. The experimental parameters are identical to those in figures 7c and 7d.

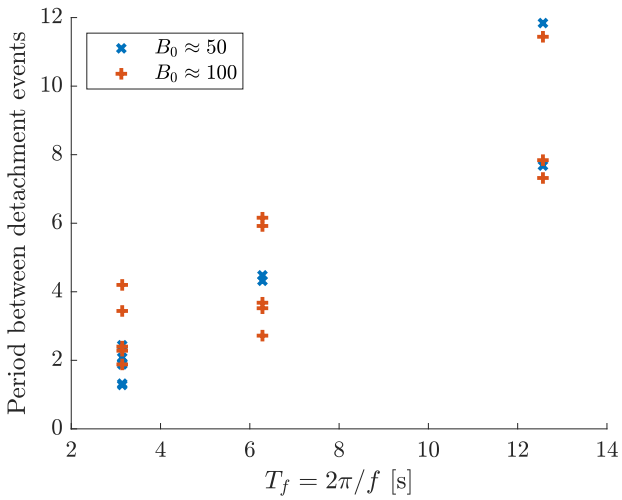

Figure 10: Scatter plot of time periods measured between detachment events against the inertial period of rotation. Only side view experiments were used to obtain these values.

5 Discussion

The results of our experiments leave many open questions for the effects of rotation and confinement on turbulent plumes. Even without the presence of rotation, the shape of the steady state formed by a point source plume along a wall is surprising. The results of a recent numerical study [7] do not appear to match the profile of close to constant width from the wall found in figure 6, and it remains important to understand this discrepancy. The difference between the numerics and our experiments may also have implications for the use of the half-cone model (6)-(8) in modelling glacial meltwater plumes. Quantifying the variation in the volume flux with height experimentally for this flow would be useful in determining whether the model can accurately represent the asymmetric plume dynamics. We only performed the non-rotating experiment at a single volume flux and source density, so there is plenty of scope for further investigation of this flow in various parameter regimes.

One caveat for our results in the non-rotating experiments is the position of the source nozzle. As discussed earlier, the dynamics near the source are thought to be dominated by the Coandă effect and the downstream impact of this is unknown. Replacing the source with a simple pipe outflow attached to the wall would remove these effects, but it is likely that the flow from this source would be laminar. Obtaining geophysically relevant parameters would be difficult in this case, but possible with a sufficiently deep tank that allows for the laminar-turbulent transition region.

The addition of rotation to the wall plume experiments resulted in frequent deviations from the steady state. The movement of the plume away from the wall and the detrainment that occurs during these detachment events has a strong impact on the amount of mixing that occurs between the plume and the ambient. Figure 11 shows the time-averaged front view of plumes at four different rotation rates for a buoyancy flux of $B_0 \approx 47.5\text{cm}^4\,\text{s}^{-3}$. Despite the difference in dye concentration between the non-rotating and rotating experiments, a clear trend is visible with the dye becoming more diffuse at higher rotation rates.

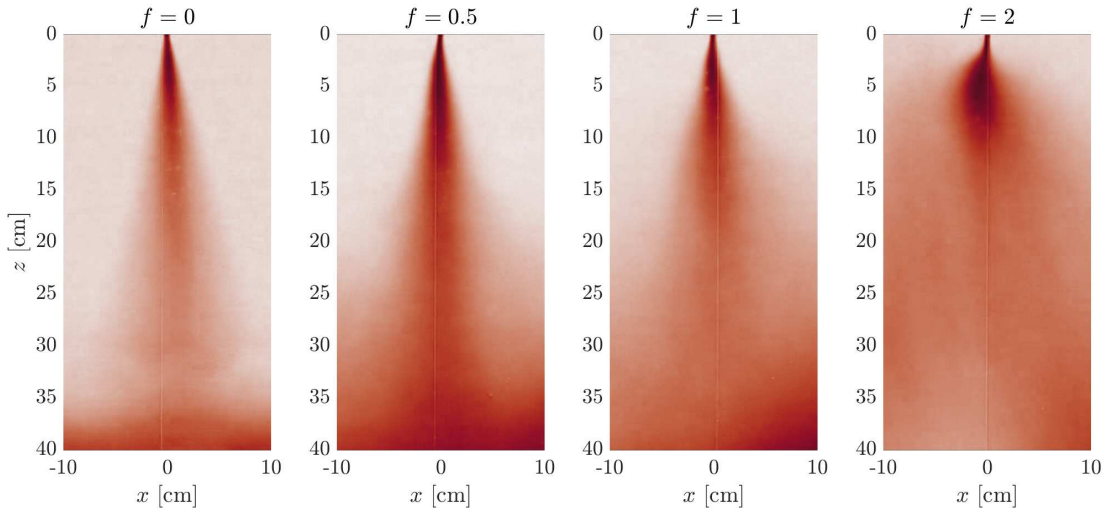

Figure 11: 3 minute time averages of the reduction in blue light intensity for four experiments in front view at various rotation rates. The time average is taken over a period that begins 20s after the start of each experiment so effects of initial transients are not seen. Note that the dye concentration in the $f = 0$ experiment is half of that in the other experiments.

The lateral spreading of dyed fluid is also greater as f increases.

This increased dispersion can be quantified by considering a Gaussian profile fit to the light intensity defecit at each height. For a given row of pixels, we fit the profile

$$I = Ae^{-\frac{(x-\mu)^2}{2\sigma^2}}, \tag{10}$$

by taking the maximum intensity deficit to be equal to A and finding the first two data points away from this maximum to have $I < A/e$, i.e. the points that are an e-folding distance from the maximum. We then assume these points are at $x = \mu \pm \sqrt{2}\sigma$, from which we obtain the mean of the Gaussian μ, and the standard deviation σ. Vertical profiles of $\sigma(z)$ provide a useful measure of dispersion to compare the different experiments with. Figure 12 plots these profiles for both the experiments shown in figure 11 and those run with a higher buoyancy flux. The profiles show a striking dependence on the rotation rate of the experiment, with the change in buoyancy flux having practically no impact on the dispersion observed. This is despite the fact that the frequency of detachment was not totally consistent between experiments with the same rotation and varying buoyancy flux.

This apparent independence of buoyancy flux for long term mixing poses an interesting question as to how wall jets without any buoyancy would develop in this rotating system. Turbulent jets initially lead to confined cylindrical structures at sufficiently high rotation

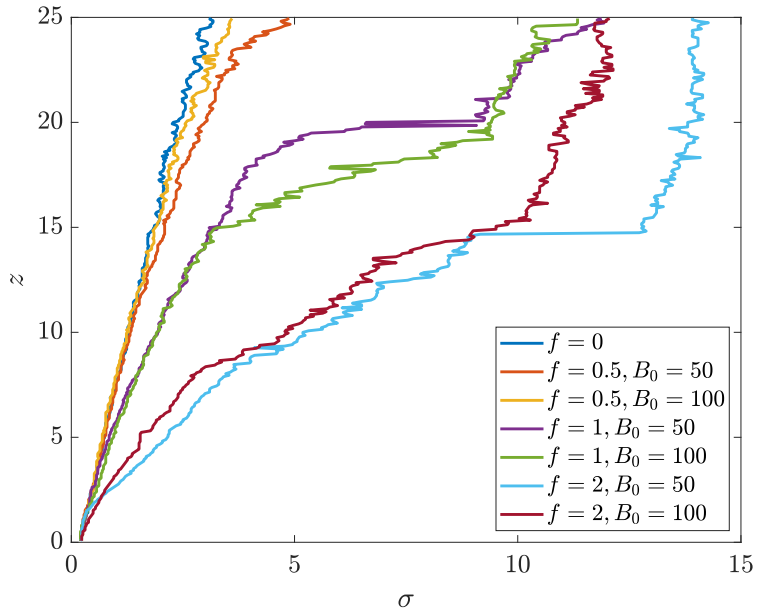

Figure 12: Plot of Gaussian standard deviation $\sigma(z)$ from 3 minute averages.

rates (see GFD Report of Lehn, 2018), but the interaction of these structures with the wall is unknown. Finding out whether a turbulent wall jet has the same detachment behaviour would be useful for further understanding the dynamics. Another process in rotating plumes found to be independent of the buoyancy flux is the precession of an axisymmetric plume in a rotating environment. The precession frequency was found in [10] to *only* rely on the rotation rate, and not the buoyancy flux of the plume or the total depth of the water. This suggests that the process of detachment from the wall may be related to the free plume precession, and gaining further insight on the wall plume dynamics could help our understanding of the laterally unconfined plumes.

The fact that the wall plume reverts to a quasi-steady state between detachment events could be indicative of bistability in the system. The existence of multiple steady states for an unconfined plume in a rotating (and stratified) environment was discovered by Deremble [6]. This study used a continuation method to numerically compute the steady states of an LES-type model where turbulent processes are parameterised by an eddy viscosity. Without rotation the method identifies the steady state solutions described by classical plume theory. Once rotation is added, a steady state similar to the classical solution is found as well as second state that exhibits very different circulation patterns. This solution has fluid *upwelling* along the vertical axis beneath the plume, and the outflow of plume fluid is deflected. If similar steady states exist for the wall plume this could explain the attachment/detachment behaviour, so a further study on steady states for this problem would provide a lot of insight into the dynamics.

The influence of the bottom boundary on the wall plume is not fully understood. At higher rotation rates the more rapid lateral spreading appears to coincide with hindered vertical motion, as can be seen in figure 11 when $f = 2$. In the video for this experiment,

detrained fluid is seen to arrange itself into Taylor columns, indicating that the Taylor–Proudman theorem is affecting the dynamics and that velocity is close to uniform with height. The combination of the bottom boundary condition and the Taylor–Proudman theorem would explain this restriction on vertical motion. However the precise effect that the bottom of the tank has on the detaching behaviour is unknown. Plume precession in [10] was found to be independent of the depth of the water, and testing whether the wall plume motion also has this property would provide further evidence to determine if the detachment is a signal of the precession.

One key result from [10] comes about because the precession is solely dependent on the rotation rate. Since precession occurs in every experiment after approximately one rotation period, rotation will always affect the dynamics as long as the source is maintained for a sufficiently long period of time. We have not quite shown that the dynamics of the wall plume are only dependent on the rotation rate, but we can hypothesise that since it is independent of the buoyancy flux similar results may apply. This would have implications for geophysical flows with sustained sources, such as glacial meltwater plumes and dense water currents running into undersea canyons. As we have seen above, plumes affected by rotation mix and disperse laterally to a greater extent than expected from a plume in a non-rotating environment, leading to changes in the long-time effects of these flows.

6 Acknowledgements

I would like to thank Craig McConnochie for advising me on this project and providing endless support, guidance and enthusiasm through the many twists and turns of my research over the summer. I would also like to thank Andrew Woods both for his series of inspiring and insightful lectures, and for the many useful discussions that helped steer my research down interesting new avenues. I am grateful too for the guidance of Claudia Cenedese, who did not let being in a different continent prevent her from providing good advice for the experiments. This summer was a phenomenal experience for me, which was in no small part down to the staff and visitors of the GFD Program. I am particularly grateful to the directors Colm Caulfield and Neil Balmforth, who helped create a wonderful atmosphere in which to do research. Finally, I want to extend my gratitude to the other Fellows on the Program, without whom this summer would not have been the same.

References

[1] W. D. Baines, *A technique for the direct measurement of volume flux of a plume*, Journal of Fluid Mechanics, 132 (1983), pp. 247–256.

[2] W. D. Baines and J. S. Turner, *Turbulent buoyant convection from a source in a confined region*, Journal of Fluid Mechanics, 37 (1969), pp. 51–80.

[3] H. C. Burridge, J. L. Partridge, and P. F. Linden, *The Fluxes and Behaviour of Plumes Inferred from Measurements of Coherent Structures within Images of the Bulk Flow*, Atmosphere - Ocean, 54 (2016), pp. 403–417.

[4] C. Cenedese and P. F. Linden, *Entrainment in two coalescing axisymmetric turbulent plumes*, Journal of Fluid Mechanics, 752 (2014), p. R2.

[5] T. Cowton, D. Slater, A. Sole, D. Goldberg, and P. Nienow, *Modeling the impact of glacial runoff on fjord circulation and submarine melt rate using a new subgrid-scale parameterization for glacial plumes*, Journal of Geophysical Research: Oceans, 120 (2015), pp. 796–812.

[6] B. Deremble, *Convective plumes in rotating systems*, Journal of Fluid Mechanics, 799 (2016), pp. 27–55.

[7] E. Ezhova, C. Cenedese, and L. Brandt, *Dynamics of Three-Dimensional Turbulent Wall Plumes and Implications for Estimates of Submarine Glacier Melting*, Journal of Physical Oceanography, 48 (2018), pp. 1941–1950.

[8] A. Fabregat Tomàs, A. C. Poje, T. M. Özgökmen, and W. K. Dewar, *Effects of rotation on turbulent buoyant plumes in stratified environments*, Journal of Geophysical Research: Oceans, 121 (2016), pp. 5397–5417.

[9] H. J. S. Fernando, R.-r. Chen, and B. A. Ayotte, *Development of a point plume in the presence of background rotation*, Physics of Fluids, 10 (1998), pp. 2369–2383.

[10] D. Frank, J. R. Landel, S. B. Dalziel, and P. F. Linden, *Anticyclonic precession of a plume in a rotating environment*, Geophysical Research Letters, 44 (2017), pp. 9400–9407.

[11] J. C. Goodman, G. C. Collins, J. Marshall, and R. T. Pierrehumbert, *Hydrothermal plume dynamics on Europa: Implications for chaos formation*, Journal of Geophysical Research, 109 (2004), p. E03008.

[12] K. R. Helfrich and T. M. Battisti, *Experiments on baroclinic vortex shedding from hydrothermal plumes*, Journal of Geophysical Research, 96 (1991), p. 12511.

[13] N. G. Hogg and H. M. Stommel, *The Heton, an Elementary Interaction Between Discrete Baroclinic Geostrophic Vortices, and Its Implications Concerning Eddy Heat-Flow*, Proceedings of the Royal Society A: Mathematical, Physical and Engineering Sciences, 397 (1985), pp. 1–20.

[14] B. E. Launder and W. Rodi, *The Turbulent Wall Jet Measurements and Modeling*, Annual Review of Fluid Mechanics, 15 (1983), pp. 429–459.

[15] P. F. Linden, G. F. Laneserff, and D. A. Smeed, *Emptying Filling Boxes - the Fluid-Mechanics of Natural Ventilation*, Journal of Fluid Mechanics, 212 (1990), pp. 309–335.

[16] J. Marshall and F. Schott, *Open-ocean convection: Observations, theory, and models*, Reviews of Geophysics, 37 (1999), pp. 1–64.

[17] C. D. McConnochie and R. C. Kerr, *The turbulent wall plume from a vertically distributed source of buoyancy*, Journal of Fluid Mechanics, 787 (2015), pp. 237–253.

[18] B. R. Morton, G. Taylor, and J. S. Turner, *Turbulent Gravitational Convection from Maintained and Instantaneous Sources*, Proceedings of the Royal Society A: Mathematical, Physical and Engineering Sciences, 234 (1956), pp. 1–23.

[19] D. A. Slater, D. N. Goldberg, P. W. Nienow, and T. R. Cowton, *Scalings for Submarine Melting at Tidewater Glaciers from Buoyant Plume Theory*, Journal of Physical Oceanography, 46 (2016), pp. 1839–1855.

[20] K. G. Speer and J. Marshall, *The growth of convective plumes at seafloor hot springs*, Journal of Marine Research, 53 (1995), pp. 1025–1057.

[21] A. W. Woods, *Turbulent Plumes in Nature*, Annual Review of Fluid Mechanics, 42 (2010), pp. 391–412.

[22] H. Yamamoto, C. Cenedese, and C. P. Caulfield, *Laboratory experiments on two coalescing axisymmetric turbulent plumes in a rotating fluid*, Physics of Fluids, 23 (2011), p. 056601.